Supporting information for

Formation of Room-Temperature $Ia\bar{3}d$ Phase Obtained for the Binary Mixture Containing Different Sizes of Siloxanyl Terminals

Yuki Kawase,[a] Shoichi Kutsumzu,[b,*] Taro Udagawa,[b] Yohei Miwa,[b] Yasuhisa Yamamura,[c] and Kazuya Saito[c]

[a]*Materials Chemistry Course, Department of Materials Science and Processing, Graduate School of Natural Science and Technology, Gifu University, Yanagido, Gifu 501-1193, Japan.*

[b]*Department of Chemistry and Biomolecular Science, Faculty of Engineering, Gifu University, Yanagido, Gifu 501-1193, Japan.*

[c]*Department of Chemistry, Faculty of Pure and Applied Sciences, University of Tsukuba, Tsukuba, Ibaraki 305-8571, Japan.*

Contents

1. Methods

1.1 Calorimetric investigation.

Phase transitions were determined by using a SII Nanotechnologies DSC7020. The measurements were performed under a dry N_2 flow of c. 40 mL min^{-1} and the scanning rate was 5 K min^{-1}.

1.2. Optical investigation.

The texture of each mesophase was observed usually under crossed polarizers using polarizing optical microscopes (POM; an Olympus BX53P) equipped with a Mettler FP82HT hotstage and a Mettler FP90 controller. The scanning rate was 5 K min^{-1}.

1.3. X-ray diffraction investigation.

X-ray diffraction (XRD) patterns at elevated temperatures were obtained for powder samples using a Rigaku NANO-Viewer Imaging Plate (IP) system. CuKα radiation (wavelength λ = 0.154 nm) at 45 kV and 60 mA was focused with a Conforcal Max-Flux mirror and collimated into the sample position in a home-made heated cell using a three-slit system. The powder sample was inserted into a drilled hole in a brass plate, sealed with two Kapton windows at both sides, which was placed in the above heated cell, and the temperature was controlled by a Rigaku ThermoPlus 2 system. The diffracted X-rays were recorded on an IP camera with an effective area of 11.5 x 11.5 cm^2 (BAS-IP SR127; 2300 × 2300 $pixel^2$). The intensities were radially integrated and averaged to produce a circularly averaged pattern using an attached software R-AXIS DS3C with a relation of $2d\sin\theta = \lambda$, where d is a Bragg spacing, 2θ being the scattering angle.

1.4. Electron density calculation.

All the detected diffraction peaks were reasonably approximated to a Gaussian line shape and so that the peak area intensities and their errors were estimated through curve fitting using the graph software Sma4Win ver. 1.54 (produced and distributed by T. Suzuki). The Lorentz correction on them yielded the final intensities. The experimental magnitude of structure factors ($|F_{obs}|$) and errors ($\sigma(F_{obs})$) thus estimated are tabulated together with the estimated ones (F_{calc}) via maximum entropy method (MEM) analyses. The reconstruction of electron density maps for the $Ia\bar{3}d$ phases was performed using the structure factors $|F_{obs}|$. The symmetry $Ia\bar{3}d$ brings the situation where the sign of one half of the structure factors belonging to general $\{hkl\}$ is opposite to that of the other half. Moreover, the Landau theory of freezing for the $Ia\bar{3}d$ phase formation[S1] requires the same signs of the structure factors for the two strongest reflections (+2,+1,+1) and (+2,+2,0). In our MEM analyses, the signs were assumed to be both –, while those of the others are automatically determined by the symmetry. The signs of the structure factors other than {211} and {220} were estimated during the optimization process between F_{obs}'s and F_{calc}'s on the basis of the MEM analyses. The analyses were performed using a laboratory-made code and the space of the unit cell was divided into 128×128×128 pixels. The detailed procedure was already published[S2,S3]. The electron density distribution for the single molecules examined was calculated quantum-mechanically on the basis of the density functional theory at the B3LYP[S4]/6-31G[S5] level using a Gaussian16 package[S6]. The obtained result is summarized in Fig. S24. This offers a clue to obtaining deeper insights from the reconstructed electron density and considering the positions of core parts in the unit cell because the electron density of hydrazine linkage (-CO-HN-NH-CO-) has the highest within the molecule for both Bis-B10Si2 and Bis-B10Si3.

We also evaluated the partial molecular volume of the central core, alkyl chain spacer, and siloxanyl terminal portions by using the Winmostar V11.2.2 software for the quantum-mechanically optimized molecular structures. The data are compiled in Table S9 and Fig. S26, revealing the chemical locations in terms of the chemical components for each binary mixture.

1.5. Infrared spectral investigation.

Fourier Transform Infrared (FT-IR) spectra were recorded using a Perkin-Elmer Spectrum 400 MIR/FIR spectrometer equipped with a home-made hotstage. A thin sample film was prepared on a KBr plate (5×5×1 mm^3) from a chloroform solution and sandwiched between two KBr plates at around 410 K in the LC state. The sample thickness was adjusted to ensure that the bands' absorbances were the Lambert–Beer law range. The temperature was controlled by an OMRON ES100P controller. The measurements were performed on the transmittance mode with 16 scans at 4 cm^{-1} optical resolution. The sample room was purged with N_2 gas.

2. Materials

The component compounds 1,2-bis(4′-(10′′-(1,1,3,3,3-pentamethyldisiloxan-1-yl)-*n*-dec-1′′-yloxy)benzoyl)hydrazine (Bis-B10Si2) and 1,2-bis(4′-(10′′-(1,1,3,3,5,5,5-heptamethyltrisiloxan-1-yl)-*n*-dec-1′′-yloxy)benzoyl)hydrazine (Bis-B10Si3) were prepared according to the literatures [S7]. Their analytical data are shown below. Polydimethylsiloxane (PDMS) was purchased from Shin-Etsu Chemical Co., Ltd. (KF-96-50cs, molecular weight 3500 g mol^{-1}).

Bis-B10Si2: ^{1}H NMR (392 MHz, $CDCl_3$) δ = 0.00 – 0.06 (m, 30H, $SiCH_3$), 0.49 (t, J = 7.4 Hz, 4H, $SiCH_2$), 1.24 – 1.34 (m, 20H, $(CH_2)_5$), 1.79 (quin, J = 7.1 Hz, 4H, CH_2CH_2O), 3.99 (t, J = 6.5 Hz, 4H, CH_2O), 6.93 (dt, J_1 = 9.4 Hz, J_2 = 2.5 Hz, 4H, Ar−H), 7.81 (dt, J_1 = 9.4 Hz, J_2 = 2.4 Hz, 4H, Ar−H), 9.13 (s, 2H, NH). Elemental Anal. Calcd for $Si_4C_{44}H_{80}N_2O_6$: C, 62.51; H, 9.54; N, 3.31. Found: C, 62.40; H, 9.82; N, 3.42 %.

Bis-B10Si3: ^{1}H NMR (392 MHz, $CDCl_3$) δ = 0.00 – 0.08 (m, 42H, $SiCH_3$), 0.51 (t, J = 7.6 Hz, 4H, $SiCH_2$), 1.24 – 1.36 (m, 20H, $(CH_2)_5$), 1.79 (quin, J = 7.1 Hz, 4H, CH_2CH_2O), 3.99 (t, J = 6.5 Hz, 4H, CH_2O), 6.92 (d, J = 8.5 Hz, 4H, Ar−H), 7.81 (d, J = 9.0 Hz, 4H, Ar−H), 9.16 (s, 2H, NH). Elemental Anal. Calcd for $Si_6C_{48}H_{92}N_2O_8$: C, 58.01; H, 9.33; N, 2.82. Found: C, 58.28; H, 9.39; N, 2.94 %.

The binary mixtures containing 3 and 10 mol% of PDMS and 30, 50, and 70 mol% of Bis-B10Si3 (denoted M-30, -50, and -70) were obtained by mixing two components in solution using acetone as the solvent. After that, the solutions were heated to around 100 °C to remove the solvent and vacuum-dried at room temperature for 5 h. They were further mixed at around 160 °C in the molten state and quenched down to room temperature by immersing the sample vials into water.

The room-temperature aging of the mixtures was conducted by the storage of the samples at 296 K in a dry atmosphere under dark in a temperature-regulated oven.

3. Thermotropic phase behaviors

3.1. POM textures

(a) 3 mol% PDMS mixture

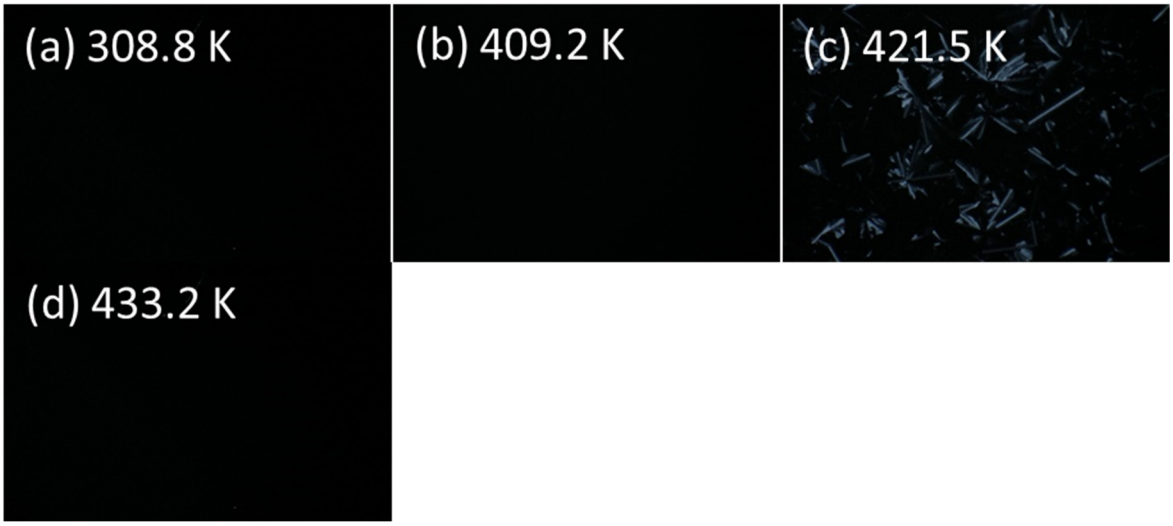

Fig. S1. Microphotographs for the mixture of Bis-B10Si2 and 3 mol% PDMS under crossed polarizers at (a) 308.8 K (Cub), (b) 409.2 K (Cub), (c) 421.5 K (Col_h), (d) 433.2 K (Iso) on cooling.

Fig. S2. Microphotographs for the mixture of Bis-B10Si2 and 3 mol% PDMS under crossed polarizers at (a) 398.2 K (Cub), (b) 423.1 K (Col_h), (c) 433.2 K (Iso) on heating.

(b) 10 mol% PDMS mixture

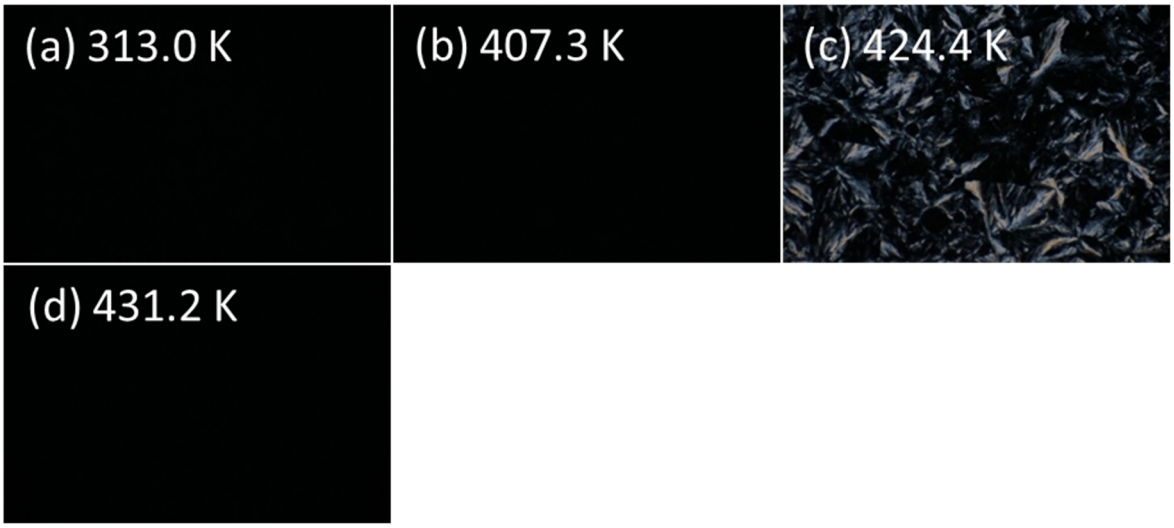

Fig. S3. Microphotographs for the mixture of Bis-B10Si2 and 10 mol% PDMS under crossed polarizers at (a) 313.0 K (Cub), (b) 407.3 K (Cub), (c) 424.4 K (Col_h), (d) 431.2 K (Iso) on cooling.

Fig. S4. Microphotographs for the mixture of Bis-B10Si2 and 10 mol% PDMS under crossed polarizers at (a) 418.8 K (around the Cub to Col_h phase transition), (b) 421.1 K (Col_h), (d) 430.2 K (Iso) on heating.

(c) M-30

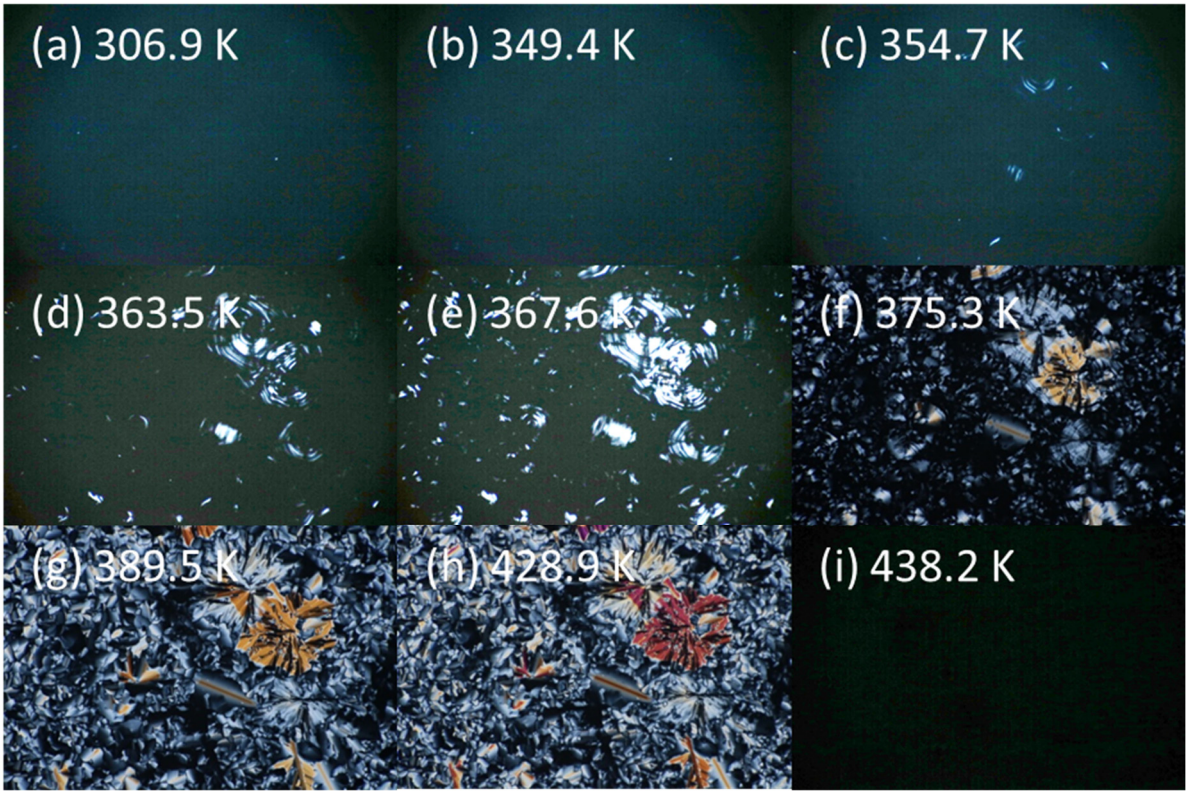

Fig. S5. Microphotographs for M-30 mixture under crossed polarizers at (a) 306.9 K (Cub), (b) 349.4 K (Cub), (c) 354.7 K (around the Col_h to Cub transition), (d) 363.5 K (Col_h), (e) 367.6 K (Col_h), (f) 375.3 K (Col_h), (g) 389.5 K (Col_h), (h) 428.9 K (Col_h), and (i) 438.2 K (Iso) on cooling. The brightness of the frames a-e and i was by 80% increased using an image software than the frames f-h.

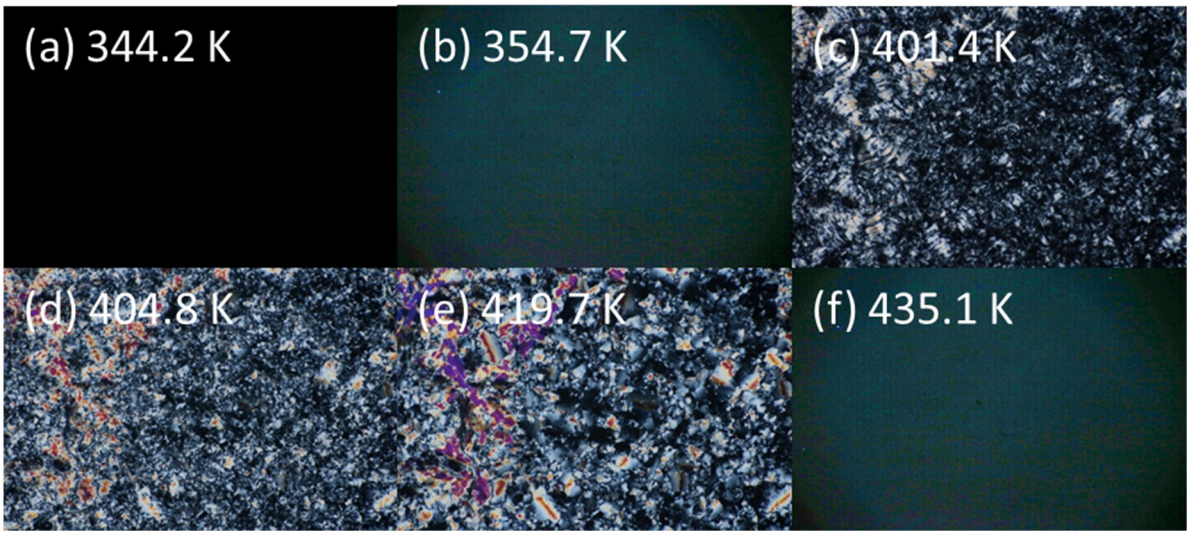

Fig. S6. Microphotographs for M-30 mixture under crossed polarizers at (a) 344.2 K (Cub), (b) 354.7 K (Cub), (c) 401.4 K (Col_h), (d) 404.8 K (Col_h), (e) 419.7 K (Col_h), and (f) 435.1 K (Iso) on heating after cooling down around room temperture. The brightness of the frames a-c and g was by 80% increased using an image software than the frames d-f.; thus, the original frame a was a dark image.

(d) M-50

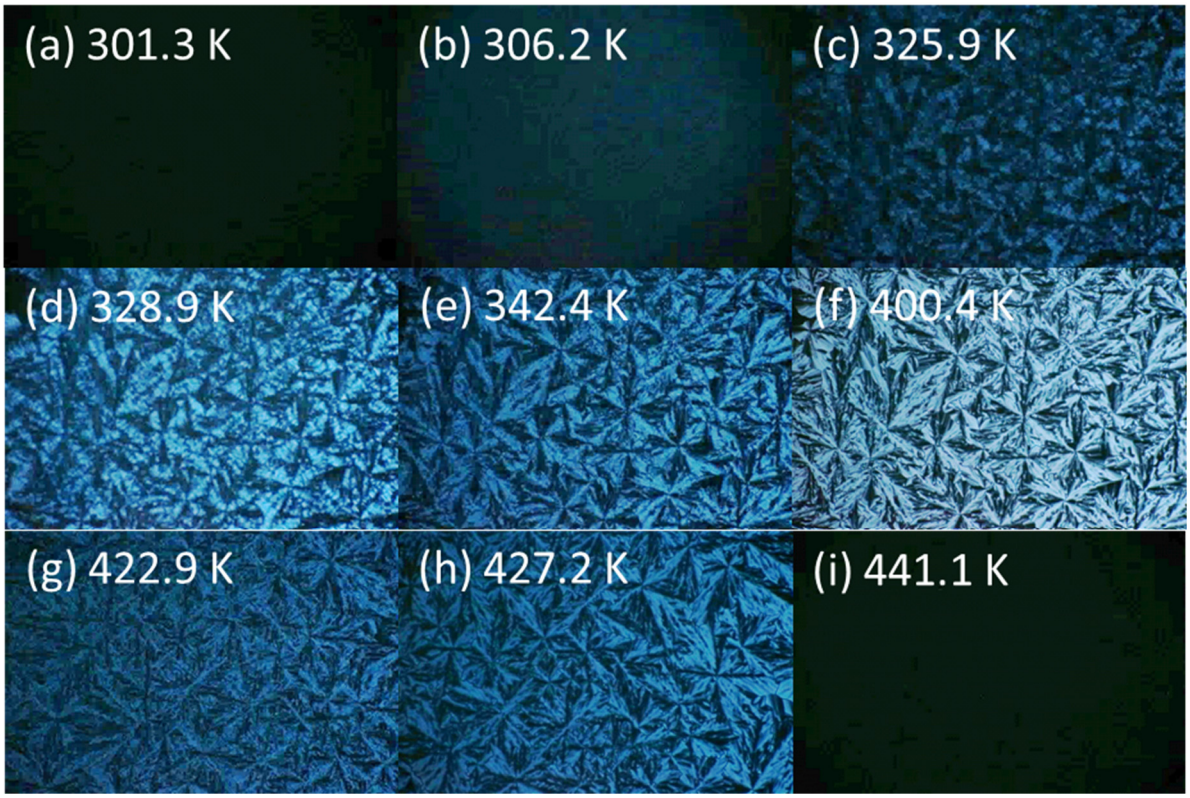

Fig. S7. Microphotographs for M-50 mixture under crossed polarizers at (a) 301.3 K (Cub), (b) 306.2 K (Cub), (c) 325.9 K (Col_r), (d) 328.9 K (Col_r), (e) 342.4 K (Col_h), (f) 400.4 K (Col_h), (g) 422.9 K (Col_h), (h) 427.2 K (Col_h), and (i) 441.1 K (Iso) on cooling. The brightness of all frames a-i was by 80% increased using an image software than their original images.

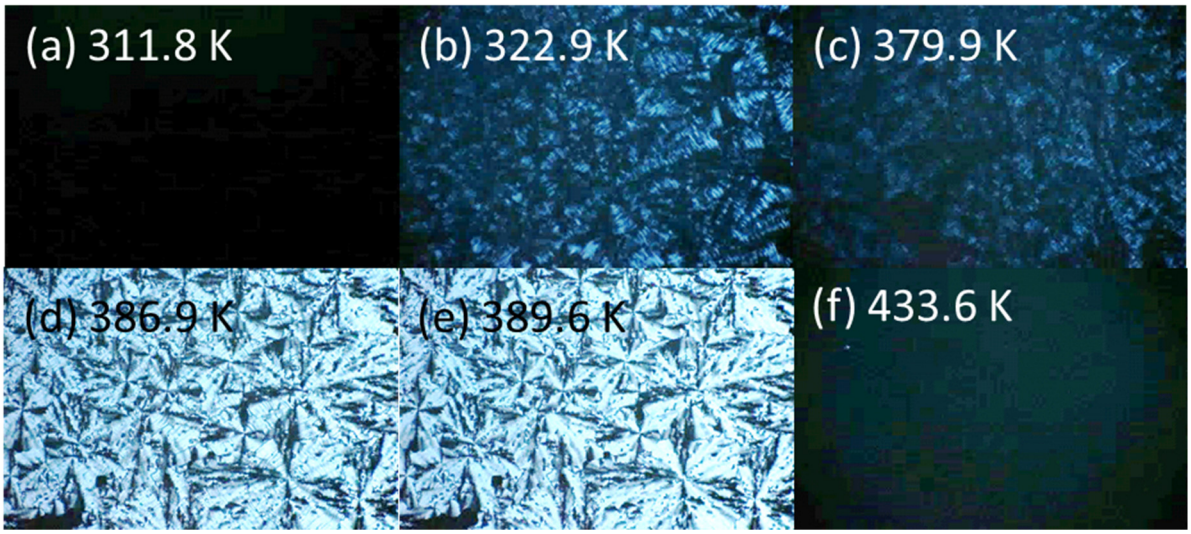

Fig. S8. Microphotographs for M-50 mixture under crossed polarizers at (a) 311.8 K (Cub), (b) 322.9 K (Col_r), (c) 379.9 K (Col_r), (d) 386.9 K (Col_h), (e) 389.6 K (Col_h), (g) 433.6 K (Iso) on heating after cooling down around room temperature. The brightness of all frames a-f was by 80% increased using an image software than their original images.

(e) M-70

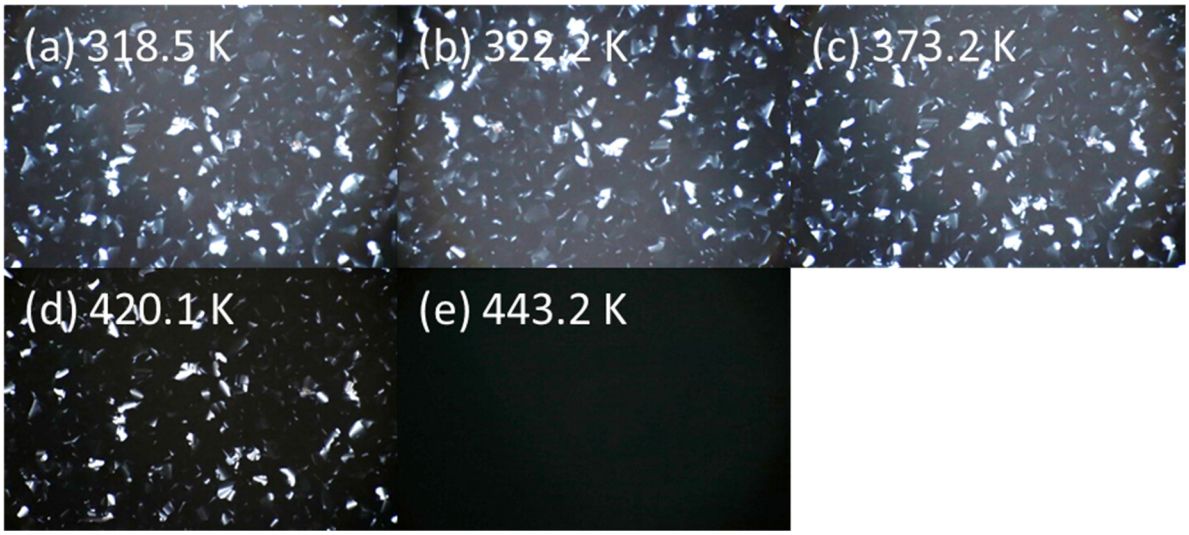

Fig. S9. Microphotographs for M-70 mixture under crossed polarizers at (a) 318.5 K (Col), (b) 322.2 K (Col), (c) 373.2 K (Col), (d) 420.1 K (Col) and (e) 443.2 K (Iso) on cooling. The brightness of all frames a-e was by 50% increased using an image software than their original images. It was difficult to differentiate the Col_{ob} and Col_{h} phases on the texture as identified by SAXS.

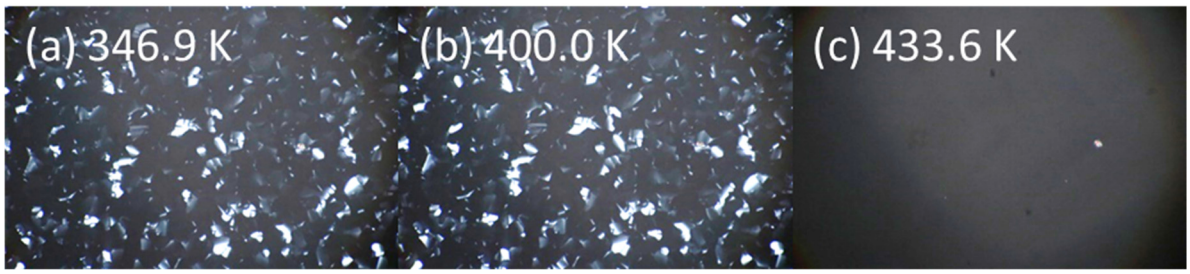

Fig. S10. Microphotographs for M-70 mixture under crossed polarizers at (a) 346.9 K (Col), (b) 400.0 K (Col), and (c) 433.6 K (Iso) on heating after cooling down around room temperature. The brightness of all frames a-c was by 50% increased using an image software than their original images.

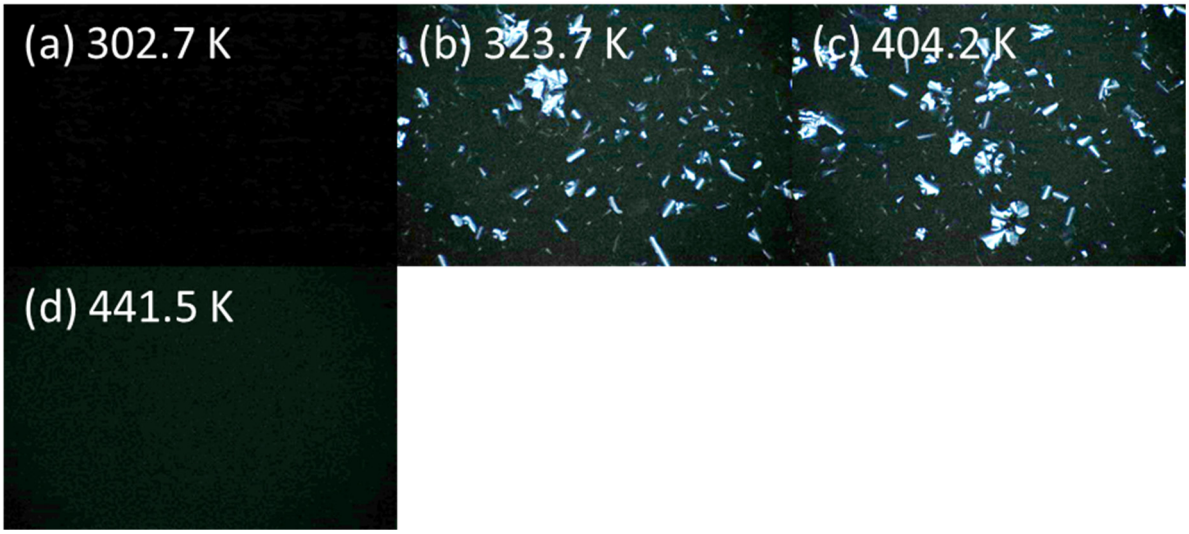

Fig. S11. Microphotographs for M-70 mixture under crossed polarizers at (a) 302.7 K (Cub), (b) 323.7 K (Col), (c) 404.2 K (Col), and (d) 441.5 K (Iso) on cooling (another observation different from Fig. S9); the frame a detected the Cub phase below the DSC exothermic peak at 297.3 K on cooling (Fig. S12). The brightness of all frames a-f was by 80% increased using an image software than their original images. It was difficult to differentiate the Col_{ob} and Col_h phases on the texture as identified by SAXS.

3.2. DSC data

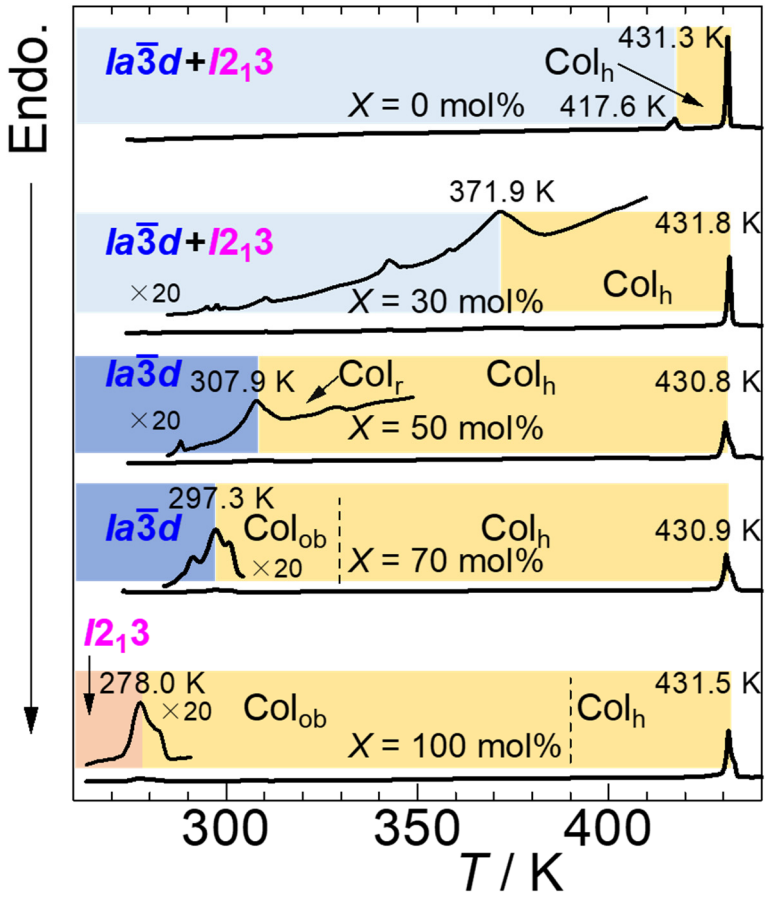

Fig. S12. DSC thermograms on cooling at 5 K min^{-1} for Bis-B10Si2, M-30, M-50, and M-70 mixtures, and Bis-B10Si3, where phase identification made by POM observation and XRD measurements is also shown; $Ia\bar{3}d$, $Ia\bar{3}d$-cubic; $I2_13$, $I2_13$-chiral cubic phase (the "$Im\bar{3}m$" type chiral Cub phase, the space group of which has recently been determined $I2_13$[S8]); Col_h, hexagonal columnar; Col_r, rectangular columnar; Col_{ob}, oblique columnar.

Table S1. Mesophases, transition temperatures (in K) and enthalpies (kJ mol^{-1} in parentheses) of two component molecules Bis-B10Si2 and Bis-B10Si3, and their mixtures (3 and 10 mol%PDMS mixtures, and M-30, -50, and -70)

Bis-B10Si2[S7]	H, after 17 days Cr 324.3 [49.1] $Ia\bar{3}d$ 422.7 [2.0] Col_h 432.3 [9.8] Iso
	C g 176 [–] $Ia\bar{3}d$ 415.8 [−1.7] Col_h 431.0 [−9.2] Iso
	2H g 188 [–] $Ia\bar{3}d$ 423.3 [2.2] Col_h 432.2 [10.4] Iso
3 mol%PDMS	C $Ia\bar{3}d$ 416.1 [−1.7] Col_h 429.1 [−10.3] Iso
	2H $Ia\bar{3}d$ 422.6 [1.7] Col_h 430.2 [9.1] Iso
10 mol%PDMS	C $Ia\bar{3}d$ 334.3 [−0.4] $Ia\bar{3}d$ + $I2_13$ 414.8 [−2.4] Col_h 428.4 [−13.2] Iso
	2H $Ia\bar{3}d$ 336.1 [0.2] $Ia\bar{3}d$ + $I2_13$ 422.8 [2.3] Col_h 429.9 [12.4] Iso
M-30	C $Ia\bar{3}d$ + $I2_13$ 371.9 [−1.7] Col_h 431.8 [−10.8] Iso
	2H $Ia\bar{3}d$ + $I2_13$ 400.9 [1.8] Col_h 432.7 [10.4] Iso
M-50	C $Ia\bar{3}d$ 307.9 [−1.1] Col_r – [–] Col_h 430.8 [−10.1] Iso
	2H $Ia\bar{3}d$ 315.7 [0.8] Col_r 385.5 [1.83] Col_h 432.3 [10.9] Iso
M-70	C $Ia\bar{3}d$ 297.3 [−2.3] Col_{ob} – [–] Col_h 430.9 [−10.9] Iso
	2H $Ia\bar{3}d$ 307.6 [4.1] Col_{ob} 369.4 [0.52] Col_h 432.7 [11.1] Iso
Bis-B10Si3[S7]	C g – [–] $I2_13$ 279.7 [−1.6] Col_{ob} ~390 [–] Col_h 430.8 [−11.4] Iso
	H g 176 [–] $I2_13$ 289.6 [1.4] Col_{ob} ~340 [–] Col_h 431.9 [11.2] Iso

Abbreviations: Cr, crystalline; g, glassy; $Ia\bar{3}d$, $Ia\bar{3}d$-cubic; $I2_13$, $I2_13$-chiral cubic (the "$Im\bar{3}m$" type chiral Cub phase, the space group of which has recently been determined $I2_13$[S8]); Col_h, hexagonal columnar; Col_r, rectangular columnar; Col_{ob}, oblique columnar.

3.3. XRD data

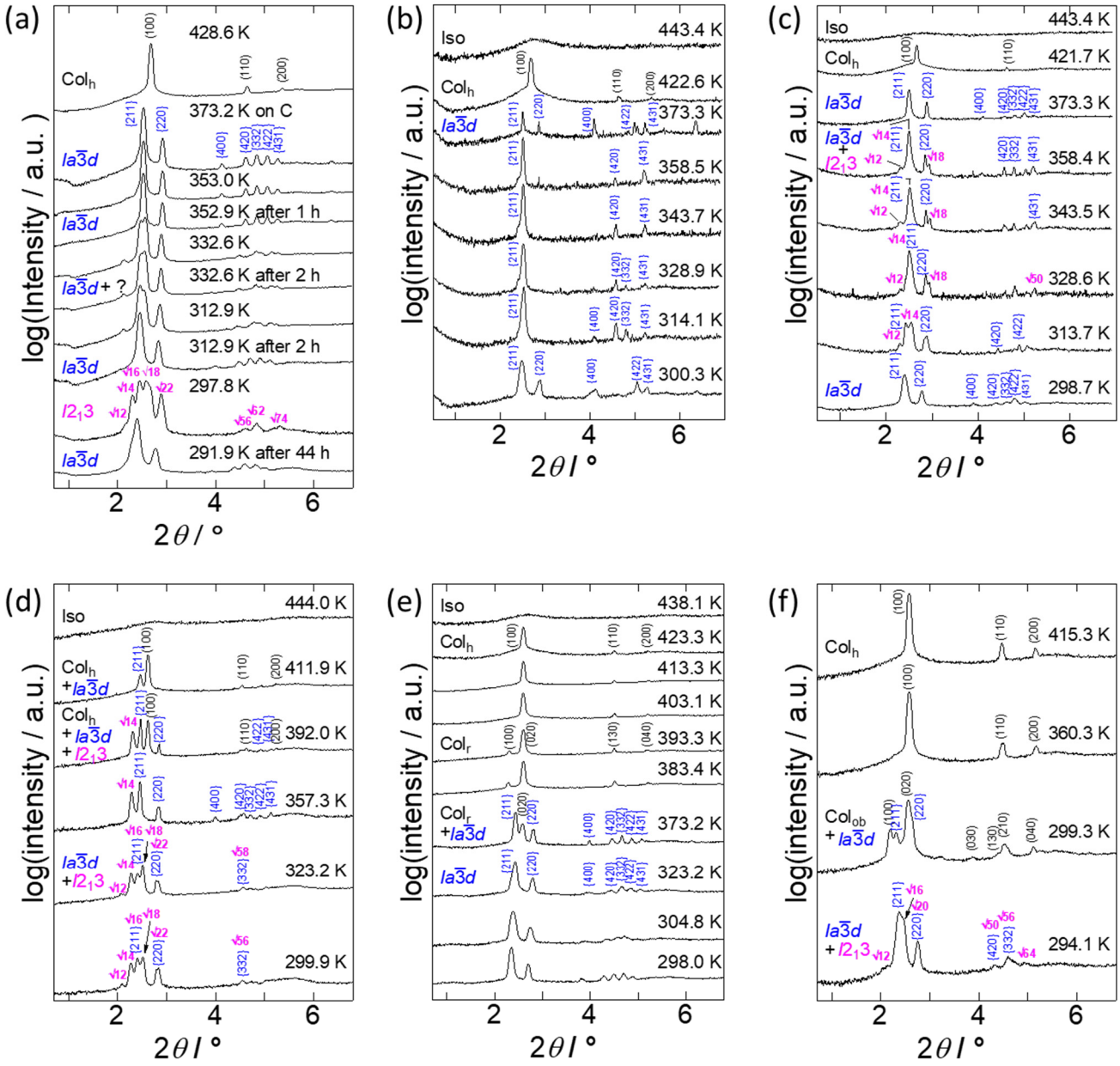

Fig. S13. Comparison of phase behaviors on cooling as monitored by XRD for (a) Bis-B10Si2, (b) 3 mol% and (c) 10 mol% PDMS mixtures, and (d) M-30, (e) M-50, and (f) M-70 mixtures. Assignments for the $I2_13$ phase are shown by square roots of numbers, not by the Miller indices.

Table S2. Experimental and calculated 2θ for the Col_{rec} phase of M-50 at 393.3 K on cooling.

Col_{rec} with a = 6.79 nm and b = 3.83 nm at 393.3 K on cooling				
(hk)	$2\theta_{obs}$ / °	$2\theta_{calc}$ / °	d_{obs} / nm	d_{calc} / nm
(10)	2.306	2.333	3.831	3.786
(02)	2.600	2.601	3.397	3.397
(13)	4.504	4.546	1.962	1.944
(04)	5.199	5.202	1.700	1.699

Table S3. Experimental and calculated 2θ for the Col_{ob} phase of M-70 at 299.3 K on cooling.

Col_{ob} with a = 4.02 nm, b = 6.90 nm, and γ = 88.8° at 299.3 K on cooling				
(hk)	$2\theta_{obs}$ / °	$2\theta_{calc}$ / °	d_{obs} / nm	d_{calc} / nm
(10)	2.196	2.196	4.023	4.023
(02)	2.562	2.562	3.448	3.448
(03)	3.864	3.843	2.287	2.299
(13)	4.386	4.386	2.015	2.015
(21)	4.536	4.550	1.948	1.942
(04)	5.106	5.125	1.731	1.724

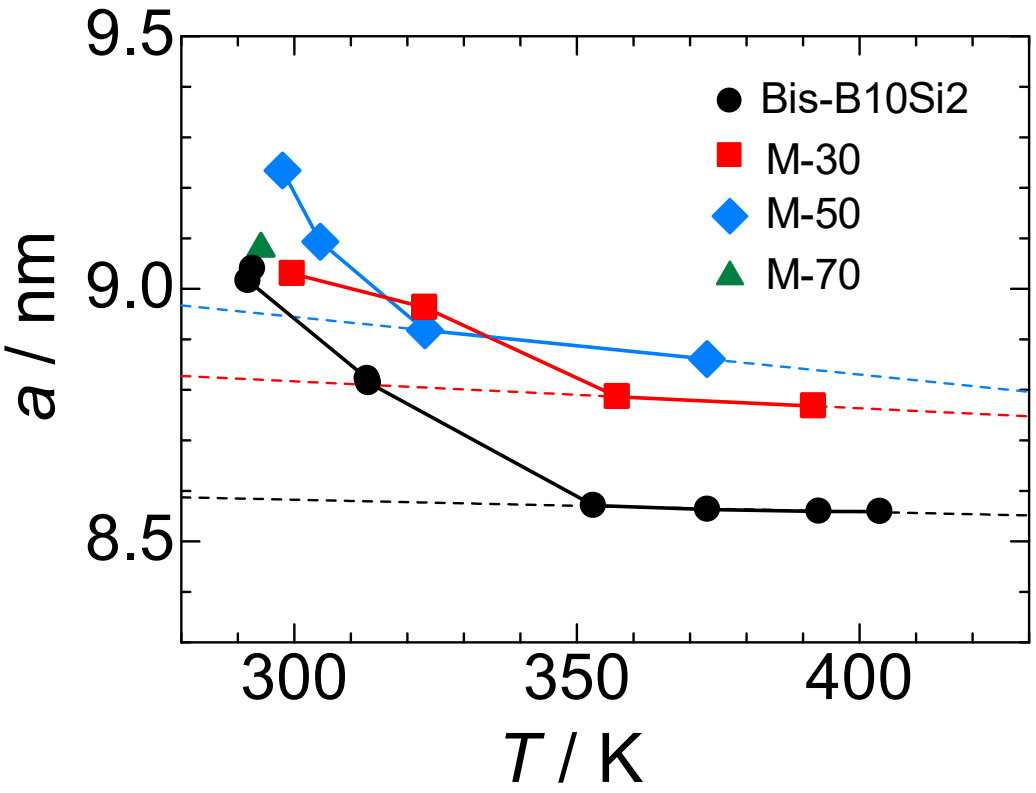

Fig. S14. Lattice dimensions of the $Ia\bar{3}d$ Cub phases as a function of temperature on cooling for Bis-B10Si2, M-30, M-50, and M-70 mixtures. For Bis-B10Si2, the $Ia\bar{3}d$ Cub phase was stabilized at 292-293 K and at 313 K after being aged for twenty hours and several hours, respectively, but not both at 323 and 333 K (see Fig. S13(a)).

4. Behaviors with Room-temperature Aging

4.1. POM textures

(a) 3 mol% PDMS mixture

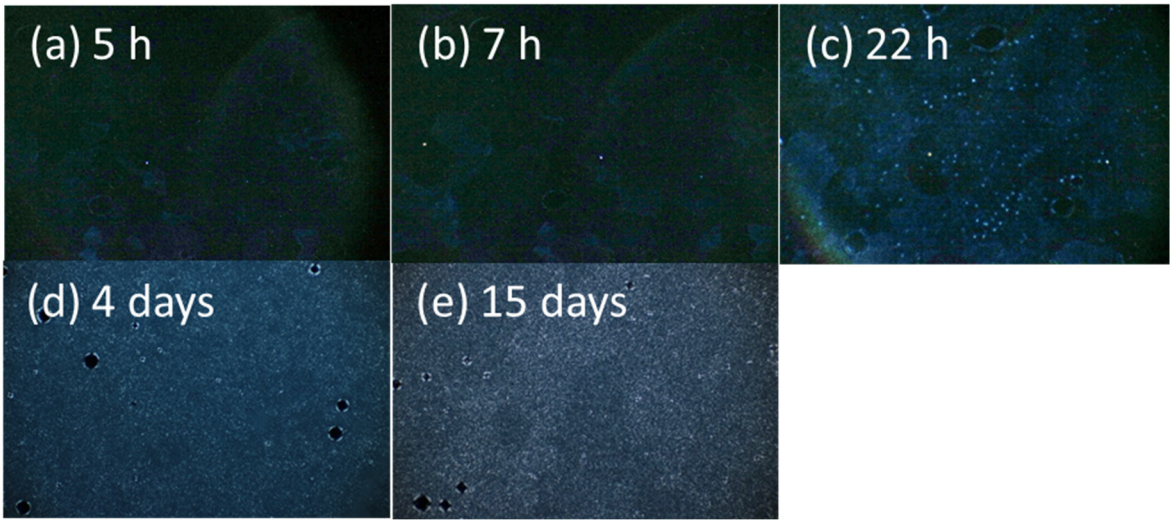

Fig. S15. Microphotographs for the 3 mol% PDMS mixture at room temperature under crossed polarizers after being aged at 296 K for (a) 5 h, (b) 7 h, (c) 22 h, (d) 4 days, and (e) 15 days. The brightness of the frames a-c was by 80% increased by using an image software than their original images to confirm whether those images are truly isotropic or not.

(b) 10 mol% PDMS mixture

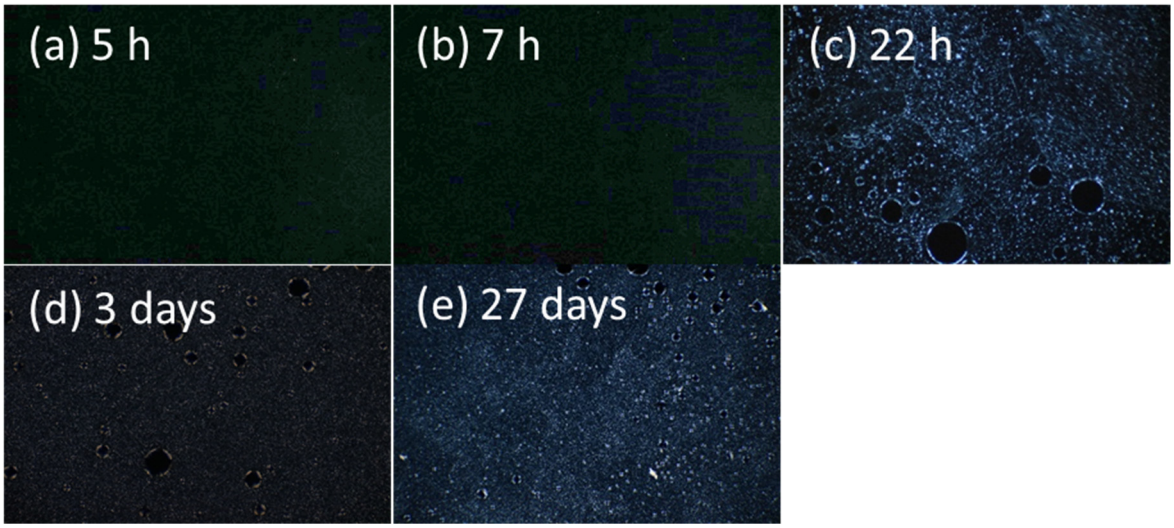

Fig. S16. Microphotographs for the 10 mol% PDMS mixture at room temperature under crossed polarizers after being aged at 296 K for (a) 5 h, (b) 7 h, (c) 22 h, (d) 3 days, and (e) 27 days. The brightness of the frames a and b was by 80% increased by using an image software than their original images to confirm whether those images are truly isotropic or not.

4.2. XRD data

Table S4. Experimental and calculated 2θ for the Col_{ob} phase of M-70 aged at room temperature for 7 days.

Col_{ob} with a = 4.15 nm, b = 7.34 nm, and γ = 91.0° aged at room temperature for 7 days				
(hk)	$2\theta_{obs}$ / °	$2\theta_{calc}$ / °	d_{obs} / nm	d_{calc} / nm
(10)	2.130	2.130	4.148	4.148
(02)	2.406	2.406	3.672	3.672
(12)	3.210	3.242	2.752	2.725
(13)	4.224	4.224	2.092	2.092
(21)	4.488	4.448	1.969	1.986
(04)	4.802	4.813	1.846	1.836

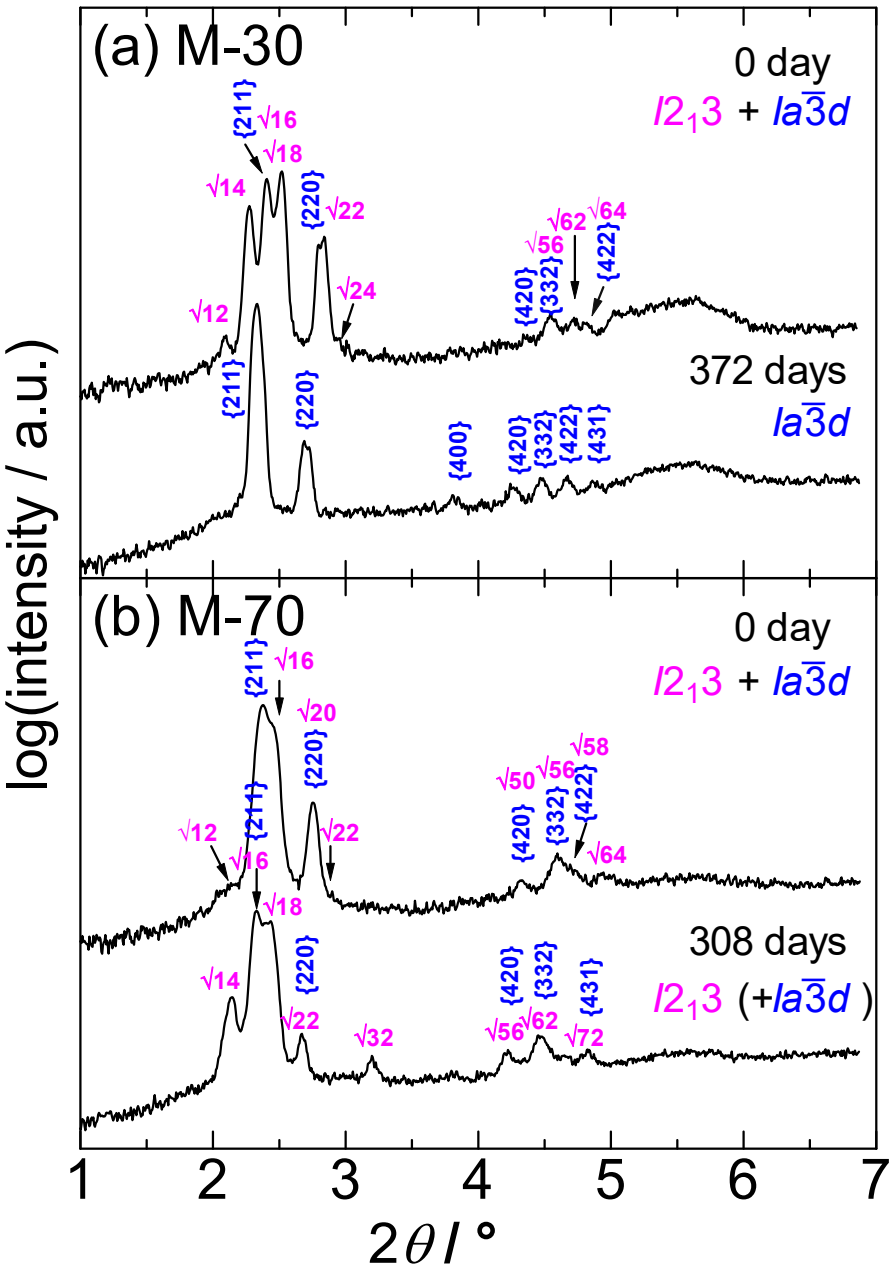

Fig. S17. SAXS patterns for (a) M-30 and (b) M-70 mixtures aged at 296 K for indicated periods. $I2_13$ indicates the "$Im\bar{3}m$" type chiral Cub phase as already explained. Details of the assignments are summarized in Tables S5-S7. The pattern of M-70 mixture aged for 308 days was characterized by $I2_13$ phase alone, although the co-existence of $Ia\bar{3}d$ phase could not be ruled out.

Table S5. Observed and calculated 2θ for the $Ia\bar{3}d$ and $I2_13$ phases of M-30 at 299.9 K immediately after cooling from the melt.

$a_{Ia\,3d}$ = 9.03±0.03 nm and a_{I2_13} = 14.67±0.04 nm				
$2\theta_{obs}$ / °	$2\theta_{calc}$ / °	d_{obs} / nm	d_{calc} / nm	Assignment
2.092	2.083	4.224	4.240	$I2_13$-√12
2.274	2.250	3.885	3.926	$I2_13$-√14
2.407	2.397	3.670	3.685	$Ia\,3d$-{211}
	2.406		3.672	$I2_13$-√16
2.517	2.552	3.511	3.462	$I2_13$-√18
2.798	2.768	3.157	3.192	$Ia\,3d$-{220}
2.839	2.821	3.112	3.132	$I2_13$-√22
2.936	2.947	3.009	2.998	$I2_13$-√24
4.341	4.377	2.036	2.019	$Ia\,3d$-{420}
4.549	4.502	1.942	1.963	$I2_13$-√56
	4.591		1.925	$Ia\,3d$-{332}
4.721	4.737	1.872	1.865	$I2_13$-√62
4.808	4.795	1.838	1.843	$Ia\,3d$-{422}
	4.813		1.836	$I2_13$-√64

Table S6. Observed and calculated 2θ for the $Ia\bar{3}d$ and $I2_13$ phases of M-70 at 294.1 K immediately after cooling from the melt.

$a_{Ia\,3d}$ = 9.08±0.03 nm and a_{I2_13} = 14.36±0.02 nm				
$2\theta_{obs}$ / °	$2\theta_{calc}$ / °	d_{obs} / nm	d_{calc} / nm	Assignment
2.135	2.131	4.138	4.145	$I2_13$-√12
2.374	2.383	3.722	3.708	$Ia\,3d$-{211}
2.460	2.461	3.591	3.590	$I2_13$-√16
2.755	2.751	3.207	3.211	$Ia\,3d$-{220}
	2.752		3.211	$I2_13$-√20
2.897	2.886	3.050	3.061	$I2_13$-√22
4.328	4.351	2.042	2.031	$Ia\,3d$-{420}
	4.351		2.031	$I2_13$-√50
4.599	4.563	1.921	1.936	$Ia\,3d$-{332}
	4.605		1.919	$I2_13$-√56
4.692	4.687	1.883	1.885	$I2_13$-√58
	4.766		1.854	$Ia\,3d$-{422}
4.928	4.923	1.793	1.795	$I2_13$-√64

Table S7. Observed and calculated 2θ for the $Ia\bar{3}d$ and $I2_13$ phases of M-70 aged at 296 K for 308 days after cooling from the melt.

$a_{Ia\,3d}$ = 9.32±0.02 nm and a_{I2_13} = 15.48±0.06 nm				
$2\theta_{obs}$ / °	$2\theta_{calc}$ / °	d_{obs} / nm	d_{calc} / nm	Assignment
2.142	2.135	4.124	4.138	$I2_13$-√14
2.334	2.282	3.785	3.871	$I2_13$-√16
	2.321		3.806	$Ia\,3d$-{211}
2.442	2.421	3.618	3.649	$I2_13$-√18
2.664	2.676	3.316	3.301	$I2_13$-√22
	2.680		3.296	$Ia\,3d$-{220}
3.198	3.228	2.763	2.737	$I2_13$-√32
4.224	4.238	2.092	2.085	$Ia\,3d$-{420}
	4.271		2.069	$I2_13$-√56
4.470	4.445	1.977	1.988	$Ia\,3d$-{332}
	4.494		1.966	$I2_13$-√62
4.824	4.833	1.832	1.829	$Ia\,3d$-{431}
	4.843		1.825	$I2_13$-√72

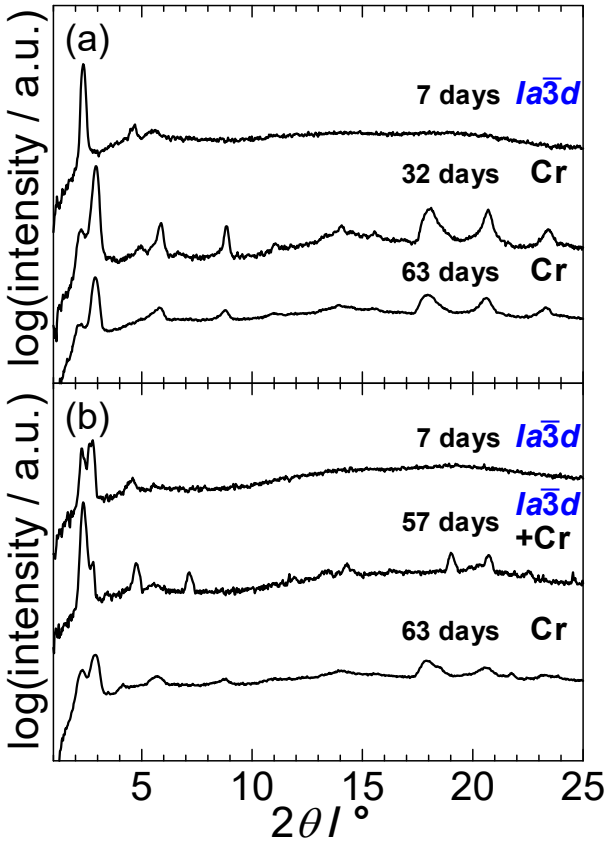

Fig. S18. XRD patterns in the wide-angle range as a function of aging period at 296 K after cooling from the melt for (a) 3 mol% and (b) 10 mol% PDMS mixtures.

4.3. IR data

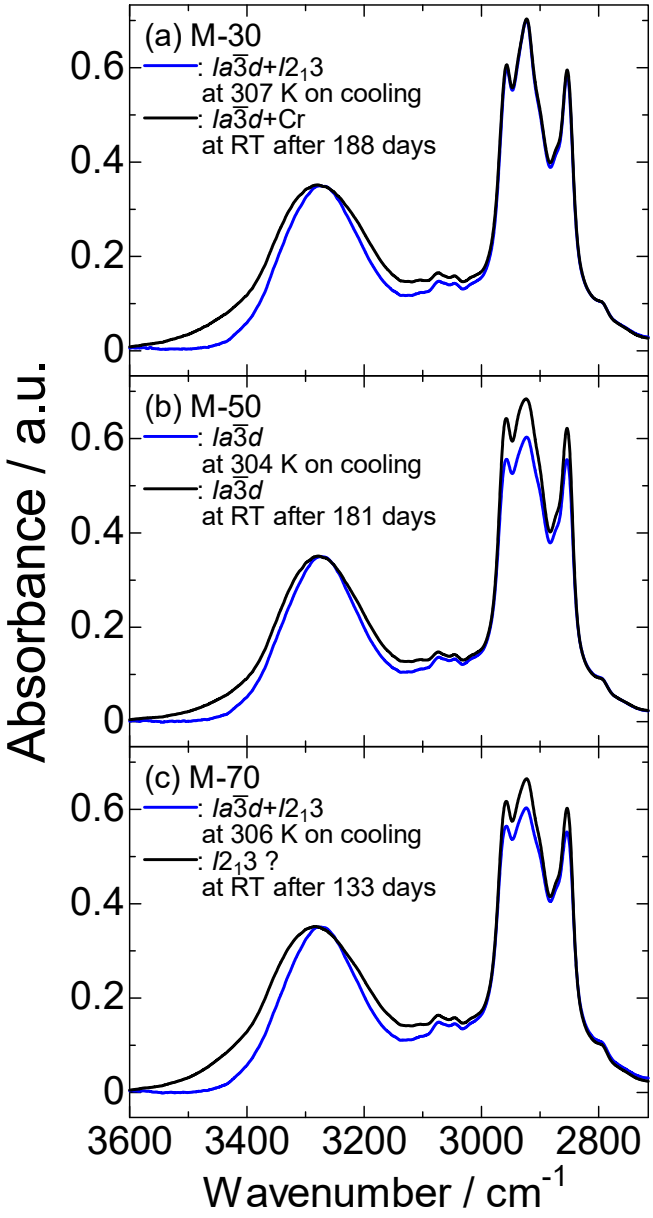

Fig. S19. Comparison of FT-IR spectra in the frequency range of 3600–2700 cm^{-1} between at around room temperature immediately after cooling and after being aged at 296 K for indicated periods for (a) M-30, (b) M-50, and (c) M-70 mixtures. In each panel, two spectral intensities are normalized with respect to the peak intensity of the ν(N–H) band. The growth of the weakly hydrogen-bonding N-H stretching component is visible in the frequency range of 3500–3400 cm^{-1}, which is related to the development of the double-layered core state[S9].

In the FT-IR studies, the following four bands are main characteristic bands to be noticed: N–H stretching (ν(N–H)), methylene C–H symmetric stretching ($\nu_s(C–H)_{CH2}$), aromatic ring C=C stretching ($\nu(C=C)_{ring}$), and symmetric Si–$(CH_3)_2$ stretching ($\nu_s(Si–C))_{Si(CH3)2}$ vibrational modes.

Fig. S20 summarizes FT-IR band frequencies as a function of aging time at room temperature (296 K) for four bands. Information on the intermolecular hydrogen bonding state of the central dicarbonylhydrazine (–C=O–NH–NH–C=O–) group is obtained from the ν(N–H) band in (a). Here, higher frequency shift corresponds to weakening of the hydrogen bonding. In Bis-B10Si2, the frequency substantially changed from 3270 to 3230 cm^{-1} after aging for 5 days, reflecting the prominent crystallization after being aged for a few days. On the other hand, the frequency of M-30 and -50 mixtures were around 3275 cm^{-1} and almost constant with aging period whereas the frequency of M-70 gradually decreased towards 3280 cm^{-1} once jumped to 3290 cm^{-1} when being aged for 5 days. For the three mixtures, however, the relatively higher frequency range around 3280 cm^{-1} was maintained during the whole aging period, reflecting a marked disturbance of crystallization in them.

Temperature behavior of the $\nu_s(C–H)_{CH2}$ band in (b) gives information on the alkyl spacer state. It is well-known that the frequency of the band is sensitively influenced by the replacement of *trans* conformers with *gauche* ones normally thermally activated on the alkyl chains, and that the increased *gauche* bond density shifts it to higher frequencies. Among the three mixtures, the highest frequency of ~2924.5 cm^{-1}, and thus, the highest flexibility of alkyl spacer, was obtained and maintained during the whole aging period for M-50.

The frequency of the $\nu(C=C)_{ring}$ band in (c) is influenced by the lateral core-core interaction and the stronger π–π interaction would shift it to lower frequencies.[S10] The samples are classified into two series, Bis-B10Si2 and three mixtures. The frequencies of the latter three moved a little bit (~0.5 cm^{-1}) to higher frequencies and then became constant with aging time, reflecting maintaining their liquid crystalline states, whereas the former's shifted to the lower frequency side owing to the crystallization.

The $\nu_s(Si–C))_{Si(CH3)2}$ band in (d) shows almost the similar trend with the behavior of the $\nu(C=C)_{ring}$ band in (c) mentioned above.

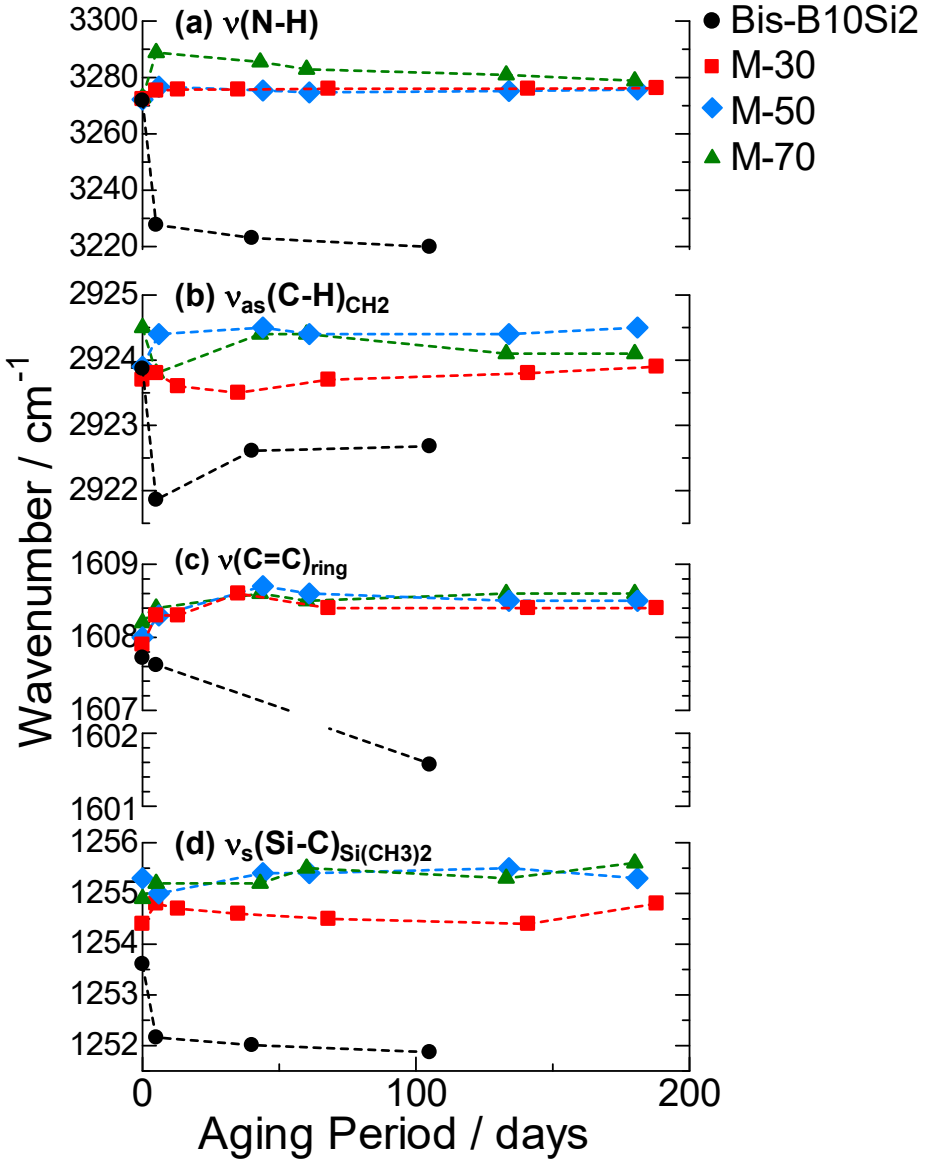

Fig. S20. FT-IR band frequencies at room temperature as a function of aging period for Bis-B10Si2 (black circles), M-30 (red squares), M-50 (blue diamonds), and M-70 mixtures (green triangles): (a) ν(N-H), (b) $\nu_{as}(C\text{-}H)_{CH2}$, (c) $\nu(C{=}C)_{ring}$ and (d) $\nu_{s}(Si\text{-}C)_{Si(CH3)2}$ vibrational modes. Note that Bis-B10Si2 crystallizes after cooling from the melt and being aged at room temperature for several days whereas the three mixtures maintain the liquid crystalline states during the whole aging period.

5. Electron density map analyses

Table S8. SAXS data of $Ia\bar{3}d$ Cub phase of M -50 mixture, measured (a) at 323 K, (b) 298 K on cooling from the melt, and (c) aged at 296 K for 378 days after the cooling (*hkl*, Miller index of respective diffraction plane; d_{obs} and d_{cal}, measured and best-fit *d*-spacings of diffraction peaks, respectively, for the q^2I vs q plots, where $q = (4\pi/\lambda)\sin\theta$ with λ and 2θ being the wavelength of the X-rays and the scattering angle, respectively; $|F_{obs}|$ and F_{cal}, observed and calculated F values, normalized to $|F_{obs}(211)|$, respectively; $\sigma(F_{cal})$, error; the (211) in the first column stands for (+2, +1, +1), for example, and $F(hkl)$ with other combinations of signs (to h, k, and l) may have an opposite sign).

a) M-50 mixture at 373 K on cooling from the melt[§]

hkl	d_{obs} / nm	d_{cal} / nm [§]	$\|F_{obs}\|$	F_{cal}	$\sigma(F_{cal})$
211	3.624	3.625	1.000	-1.000	0.009
220	3.148	3.139	0.472	-0.465	0.021
321	2.375	2.373	0.021	-0.027	0.018
400	2.218	2.220	0.236	-0.201	0.015
420	1.981	1.986	0.207	0.205	0.008
332	1.895	1.893	0.241	-0.241	0.008
422	1.816	1.813	0.188	-0.187	0.008
431	1.738	1.741	0.131	-0.122	0.012
620	1.403	1.404	0.124	0.024	0.045

[§] $a = 8.880 \pm 0.007$ nm

b) M-50 mixture at 323 K on cooling from the melt[§]

hkl	d_{obs} / nm	d_{cal} / nm [§]	$\|F_{obs}\|$	F_{cal}	$\sigma(F_{cal})$
211	3.637	3.644	1.000	-1.000	0.023
220	3.161	3.155	0.428	-0.433	0.010
321	2.416	2.385	0.024	-0.032	0.013
400	2.228	2.231	0.227	0.145	0.016
420	1.997	1.996	0.151	0.149	0.009
332	1.897	1.903	0.232	-0.233	0.006
422	1.826	1.822	0.195	-0.197	0.005
431	1.754	1.750	0.096	-0.097	0.005
521	1.621	1.629	0.022	-0.022	0.003
440	1.585	1.578	0.072	0.051	0.016

[§] $a = 8.925 \pm 0.007$ nm

c) M-50 mixture at 298 K on cooling from the melt[§]

hkl	d_{obs} / nm	d_{cal} / nm [§]	$\|F_{obs}\|$	F_{cal}	$\sigma(F_{cal})$
211	3.759	3.765	1.000	-1.000	0.008
220	3.264	3.260	0.501	-0.500	0.005
321	2.498	2.465	0.020	-0.021	0.006
400	2.309	2.305	0.238	-0.148	0.014
420	2.061	2.062	0.182	0.182	0.005
332	1.965	1.966	0.221	-0.221	0.004
422	1.880	1.882	0.240	-0.238	0.005
431	1.810	1.809	0.110	0.108	0.006
521	1.682	1.684	0.026	0.022	0.009
620	1.458	1.458	0.035	-0.032	0.006
543	1.309	1.304	0.066	0.062	0.010

[§] $a = 9.222 \pm 0.005$ nm

d) M-50 mixture aged at 296 K for 378 days after cooling from the melt[§]

hkl	d_{obs} / nm	d_{cal} / nm [§]	$\|F_{obs}\|$	F_{cal}	$\sigma(F_{cal})$
211	3.807	3.808	1.000	-1.000	0.008
220	3.299	3.297	0.458	-0.458	0.004
321	2.502	2.492	0.015	-0.024	0.008
400	2.334	2.331	0.254	-0.184	0.010
420	2.085	2.085	0.170	0.168	0.004
332	1.988	1.988	0.274	-0.274	0.003
422	1.903	1.904	0.237	-0.235	0.004
431	1.828	1.829	0.117	-0.116	0.004
521	1.701	1.703	0.022	0.024	0.009
620	1.475	1.475	0.027	0.024	0.010
541	1.434	1.439	0.013	-0.015	0.013
631	1.375	1.375	0.040	-0.038	0.012
444	1.346	1.346	0.036	0.041	0.007
543	1.320	1.319	0.051	0.054	0.008

[§] $a = 9.327 \pm 0.002$ nm

e) Bis-B10Si2 at 292K after cooling from the melt and being aged at 296 K for 44 h[§]

hkl	d_{obs} / nm	d_{cal} / nm [§]	$\|F_{obs}\|$	F_{cal}	$\sigma(F_{cal})$
211	3.684	3.681	1.000	-1.000	0.006
220	3.190	3.187	0.456	-0.442	0.012
321	2.435	2.410	0.033	-0.032	0.006
400	2.254	2.254	0.116	-0.081	0.011
420	2.015	2.016	0.173	0.173	0.003
332	1.924	1.922	0.257	-0.256	0.003
422	1.838	1.840	0.250	-0.243	0.006
431	1.767	1.768	0.112	-0.112	0.004

[§] $a = 9.016 \pm 0.003$ nm

f) M-30 mixture at 357 K on cooling from the melt[§]

hkl	d_{obs} / nm	d_{cal} / nm [§]	$\|F_{obs}\|$	F_{cal}	$\sigma(F_{cal})$
211	3.592	3.595	1.000	-1.000	0.020
220	3.116	3.113	0.530	-0.527	0.019
321	ND	2.353			
400	2.211	2.201	0.421	-0.340	0.022
420	1.965	1.969	0.282	0.283	0.009
332	1.874	1.877	0.280	-0.239	0.019
422	1.800	1.797	0.221	-0.220	0.009
431	1.724	1.727	0.171	-0.171	0.008
611	1.429	1.428	0.093	0.086	0.019
532	1.429	1.428	0.093	0.084	0.019
620	1.400	1.392	0.092	-0.089	0.014

[§] $a = 8.806 \pm 0.008$ nm

g) M-70 mixture at 343 K on cooling from the melt[§]

hkl	d_{obs} / nm	d_{cal} / nm [§]	$\|F_{obs}\|$	F_{cal}	$\sigma(F_{cal})$
211	3.664	3.666	1.000	-1.000	0.011
220	3.178	3.175	0.462	-0.462	0.008
321	2.391	2.400	0.015	-0.016	0.005
400	2.245	2.245	0.309	-0.261	0.012
420	2.008	2.008	0.201	0.194	0.008
332	1.914	1.914	0.305	-0.306	0.006
422	1.832	1.833	0.232	-0.224	0.008
431	1.761	1.761	0.115	-0.114	0.008
521	1.645	1.639	0.055	0.055	0.003
611	1.457	1.457	0.100	0.079	0.013
532	1.457	1.457	0.100	0.079	0.013
620	1.421	1.420	0.046	-0.045	0.007
631	1.333	1.324	0.048	-0.050	0.010

[§] $a = 8.979 \pm 0.002$ nm

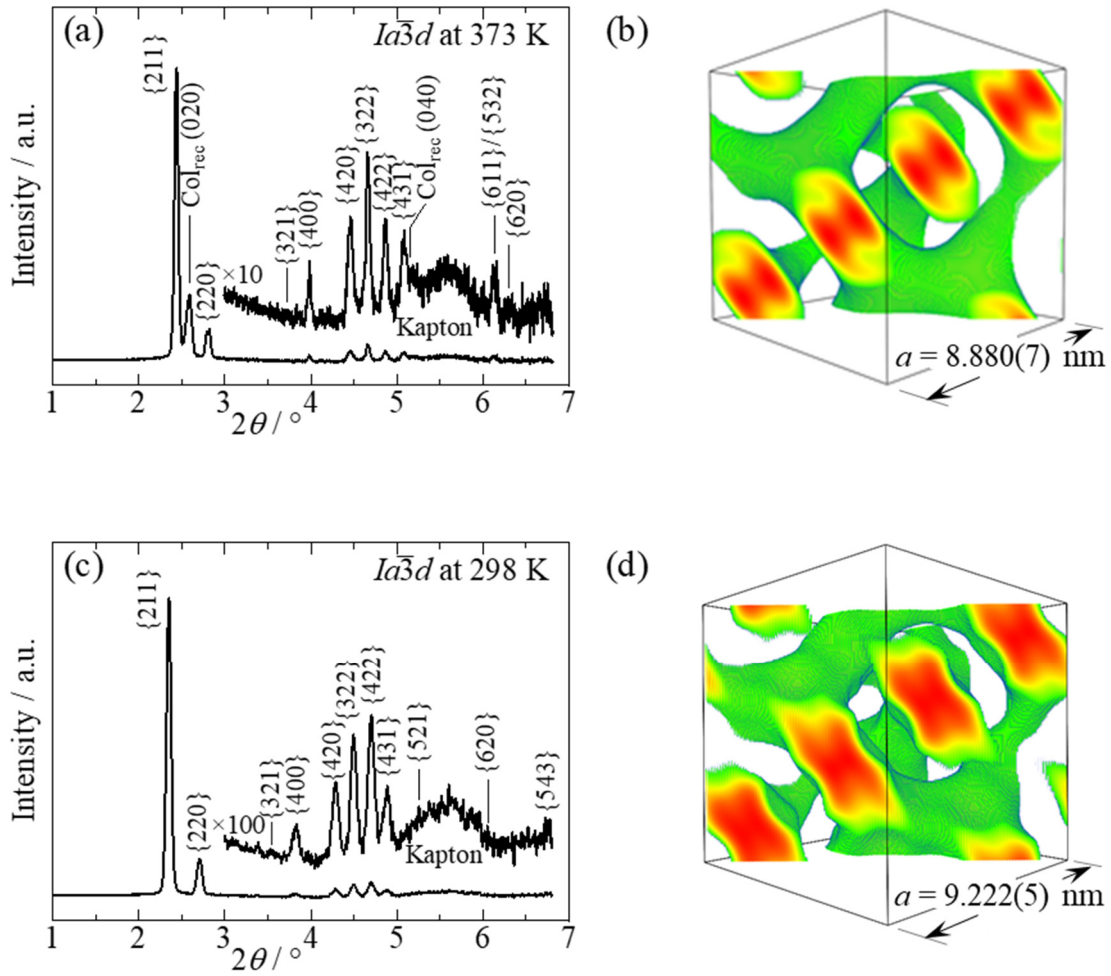

Fig. S21. (a, c) The XRD pattern and (b, d) electron density maps reconstructed from the intensity analysis for M-50 mixture (a, b) at 373 K and (c, d) at 298 K on cooling from the melt; in (b) and (d), electron density is that along the body diagonal of the unit cell [green (medium) to red (high)], where the region with a lower density than the average is shown transparent.

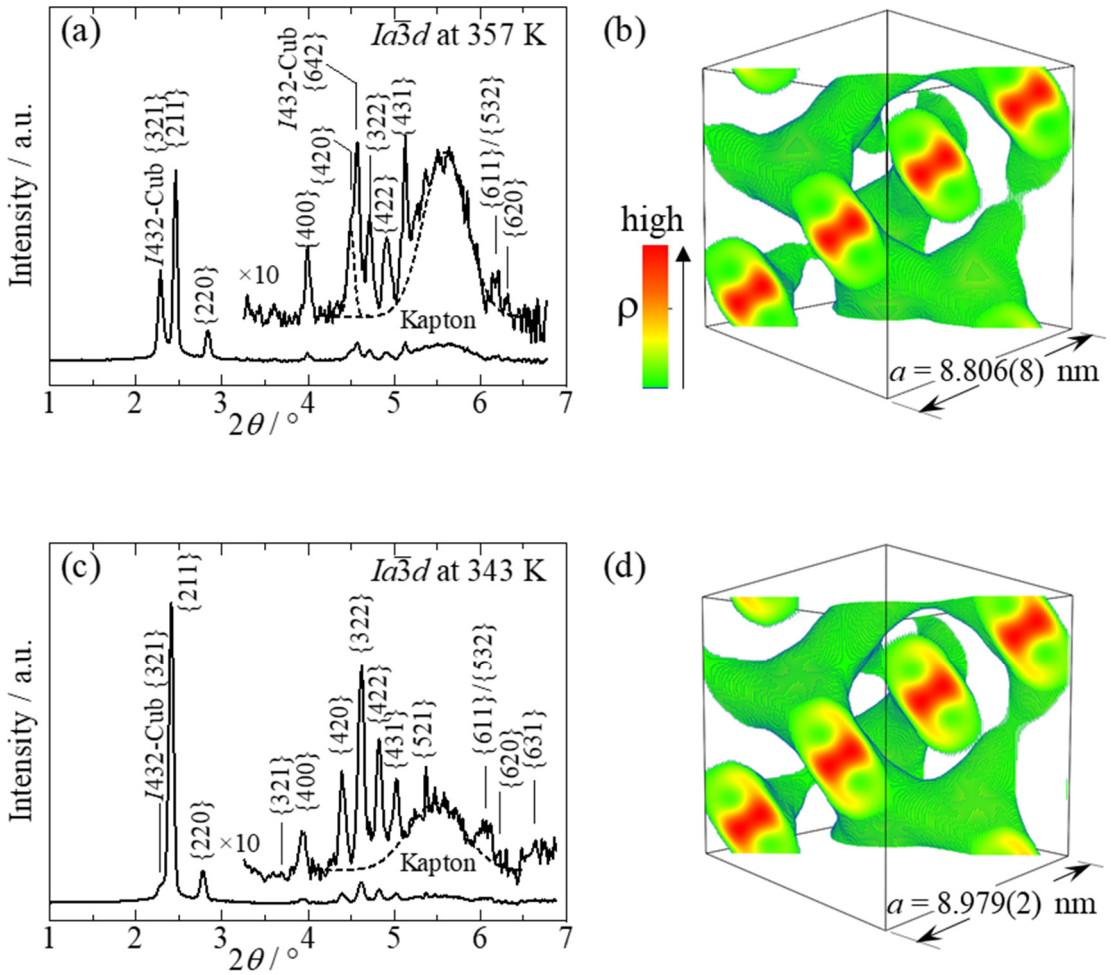

Fig. S22. (a, c) The XRD pattern and (b, d) electron density maps reconstructed from the intensity analysis for (a, b) M-30 mixture at 357 K and (c, d) M-70 mixture at 343 K on cooling from the melt; in (b) and (d), electron density is that along the body diagonal of the unit cell [green (medium) to red (high)], where the region with a lower density than the average is shown transparent.

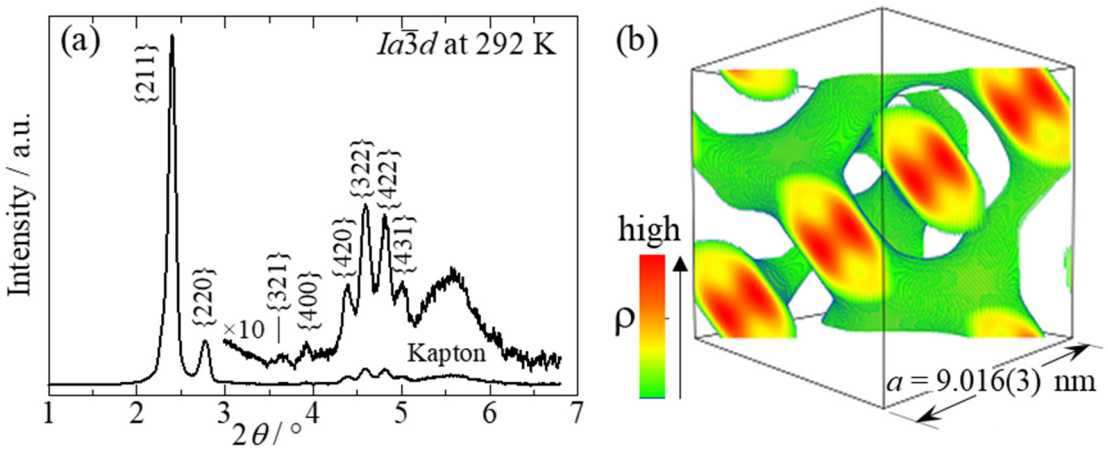

Fig. S23. (a) The XRD pattern and (b) electron density maps reconstructed from the intensity analysis for Bis-B10Si2 recorded at 292K after cooling from the melt and being aged at 296 K for 44 h. In (b), electron density is that along the body diagonal of the unit cell [green (medium) to red (high)], where the region with a lower density than the average is shown transparent.

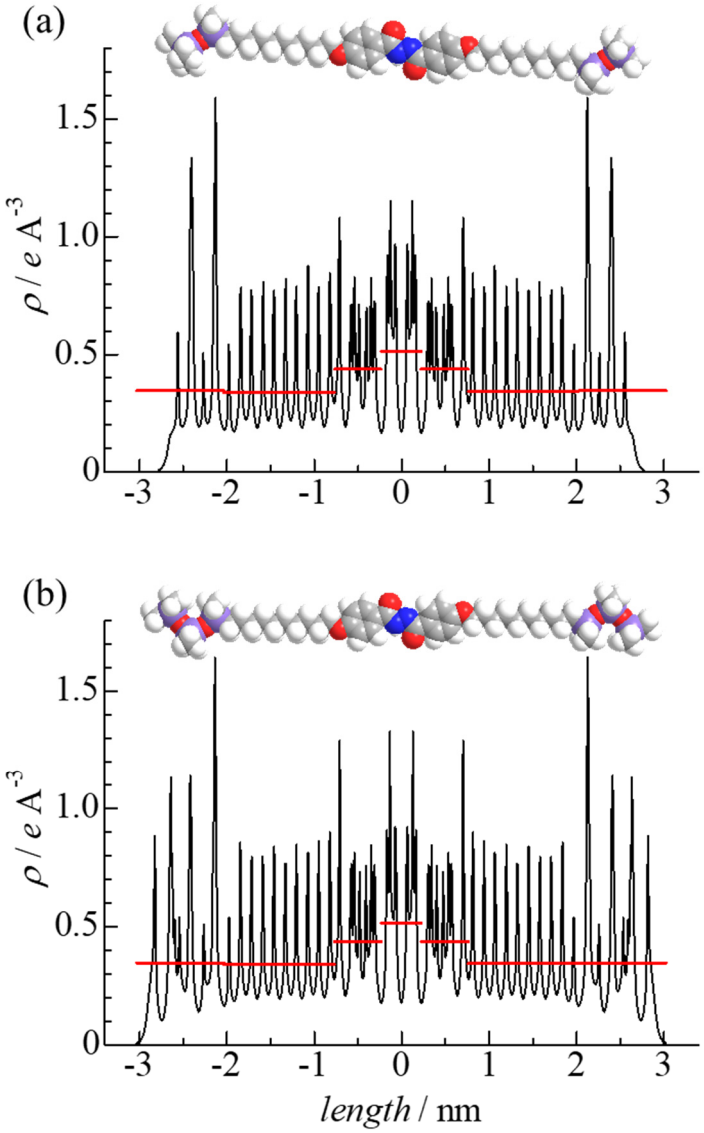

Fig. S24. Two component molecules, (a) Bis-B10Si2 and (b) Bis-B10Si3. In each frame, (top) molecular shape optimized and (bottom) electron density map integrated within a plane normal to the molecular long axis (sold curve) and its step approximation (red horizontal lines), both of which were obtained from the quantum chemical (DFT) calculation by Gaussian16 at B3LYP/6-31G* level. Note that the highest density region is dicarbonyl hydrazine linkage in both cases.

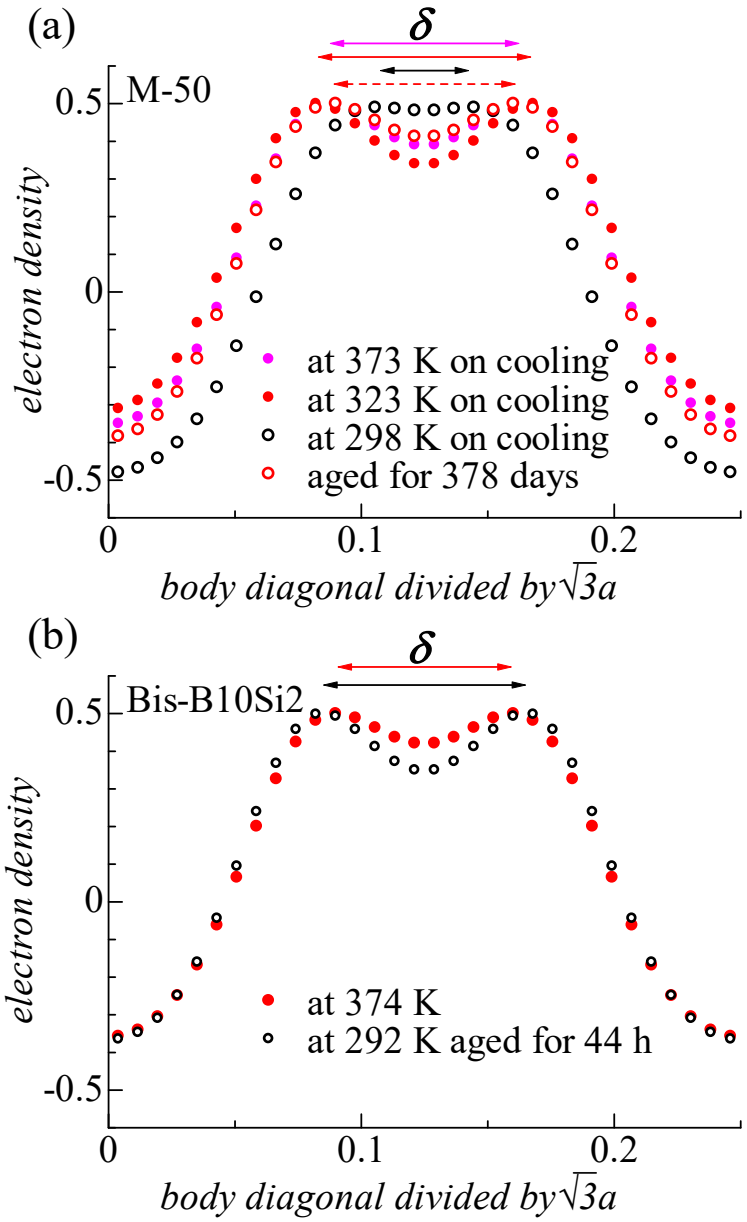

Fig. S25. Electron density along the body diagonal of the unit cell, where only 1/4 part is displayed; (a) M-50 and (b) Bis-B10Si2[S7]. The δ denotes the separation distance between split maxima for each sample under indicated conditions.

Table S9. Structural parameters of $Ia\bar{3}d$ and Col$_h$ phases in the mixtures of Bis-B10Si2 with PDMS or Bis-B10Si3.

Compd/Mixture	Nominal Si content in the terminal	[a] Molecular core volume / nm^3 (Core volume fraction)	[a] Molecular alkyl volume / nm^3 (Alkyl volume fraction)	[a] Molecular siloxanyl volume / nm^3 (Siloxane volume fraction)	$a(Ia\bar{3}d)$ / nm with measured temperature in parenthesis	[b] Number of core portions per cell, N_{cell}	[c] Number of core portions per 0.46-nm thick network column slice, N_{slice}	Average core displacement within column δ / nm	$a(Ia\bar{3}d)$ / nm with measured temperature in parenthesis	[b] Number of core portions per cell, N_{cell}	[c] Number of core portions per 0.46-nm thick column slice, N_{cell}	Average core displacement within column δ / nm	a(Col$_h$) / nm with measured temperature in parenthesis	[d] Number of core portions per 0.46-nm thick column slice, N_{slice}
Bis-B10Si 2	Si2	215.5 (0.26)	309.0 (0.37)	299.9 (0.36)	8.61 (374 K)	455	2.9	1.0	9.02 (292 K)	522	3.1	1.2	3.803 (410 K)	4.1
Mixture series 1														
2.7 mol%PDMS	Si2.6	215.5 (0.24)	309.0 (0.34)	388.3 (0.43)	8.66 (373 K)	463	2.9						3.810 (423 K)	4.1
9.9 mol%PDMS	Si4.1	215.5 (0.18)	309.0 (0.26)	658.2 (0.56)	8.65 (373 K)	461	2.9						3.831 (422 K)	4.2
Mixture series 2														
31 mol%Bis-B10Si3	Si2.3	215.5 (0.25)	309.0 (0.36)	341.9 (0.39)	8.806 (357 K)	461	2.8	1.0	9.03 (300 K)	498	3.0		3.897 (412 K)	4.1
50 mol%Bis-B10Si3	Si2.5	215.5 (0.24)	309.0 (0.35)	368.9 (0.41)	8.880 (373 K)	458	2.8	1.2	9.22 (298 K)	513	3.0	0.6	3.919 (413 K)	4.0
70 mol%Bis-B10Si3	Si2.7	215.5 (0.23)	309.0 (0.34)	395.4 (0.43)	8.979 (343 K)	459	2.8	0.9	9.08 (294 K)	475	2.8		3.956 (415 K)	4.0
Bis-B10Si3	Si3	215.5 (0.22)	309.0 (0.32)	436.7 (0.45)									4.029 (412 K)	3.9

[a] Molecular moiety volume calculated by using both Winmostar V11.2.2 and Gaussian16 at B3LYP/6-31G level.

[b] $N_{cell} = [a(Ia\bar{3}d)]^3 \times 1\ g\ cm^{-3}/[M/N_A]$, where $a(Ia\bar{3}d)$ is the cell dimension of the $(Ia\bar{3}d)$ phase, M is the molar mass of the compound/mixture per core portion, and N_A is Avogadro's number.

[c] $N_{slice} = [N_{cell}/24]/[(a(Ia\bar{3}d)/\sqrt{8})/0.46\ nm]$, where $a(Ia\bar{3}d)/\sqrt{8}$ and $N/24$ are the length of the network segments between the neighboring 3-way junctions and the number of core portions per the network segment, respectively.

[d] $N_{slice} = [(\sqrt{3})/2)\times(a(Col_h))^2 \times 0.46\ nm \times 1\ g\ cm^{-3}]/[M/N_A]$, where a(Col$_h$) is the cell dimension of the Col$_h$ phase, and M and N_A are the same as above.

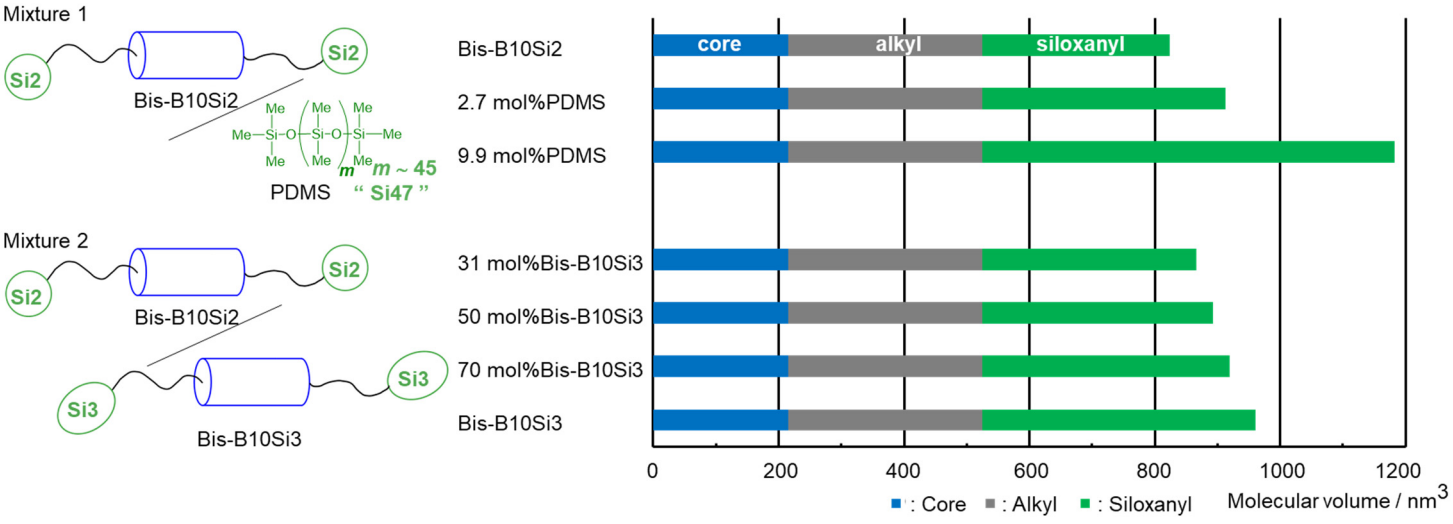

Fig. S26. Mixture characteristics in terms of molecular moiety volumes.

References in this SI

[S1] K. Saito, Y. Yamamura and S. Kutsumizu, *J. Phys. Soc. Jpn.* **2008**, *77*, 093601.

[S2] K. Ozawa, Y. Yamamura, S. Yasuzuka, H. Mori, S. Kutsumizu and K. Saito, *J. Phys. Chem. B* **2008**, *112*, 12179-12181.

[S3] Y. Nakazawa, Y. Yamamura, S. Kutsumizu and K. Saito, *J. Phys. Soc. Jpn.* **2012**, *81*, 094601.

[S4] A. D. Becke, *J. Chem. Phys.*, 1993, **98**, 5648-5652.

[S5] W. J. Hehre, R. Ditchfield and J. A. Pople, *J. Chem. Phys.*, 1972, **56**, 2257-2261.

[S6] Revision A.03, M. J. Frisch, G. W. Trucks, H. B. Schlegel, G. E. Scuseria, M. A. Robb, J. R. Cheeseman, G. Scalmani, V. Barone, G. A. Petersson, H. Nakatsuji, X. Li, M. Caricato, A. V. Marenich, J. Bloino, B. G. Janesko, R. Gomperts, B. Mennucci, H. P. Hratchian, J. V. Ortiz, A. F. Izmaylov, J. L. Sonnenberg, D. Williams-Young, F. Ding, F. Lipparini, F. Egidi, J. Goings, B. Peng, A. Petrone, T. Henderson, D. Ranasinghe, V. G. Zakrzewski, J. Gao, N. Rega, G. Zheng, W. Liang, M. Hada, M. Ehara, K. Toyota, R. Fukuda, J. Hasegawa, M. Ishida, T. Nakajima, Y. Honda, O. Kitao, H. Nakai, T. Vreven, K. Throssell, J. A. Montgomery, Jr., J. E. Peralta, F. Ogliaro, M. J. Bearpark, J. J. Heyd, E. N. Brothers, K. N. Kudin, V. N. Staroverov, T. A. Keith, R. Kobayashi, J. Normand, K. Raghavachari, A. P. Rendell, J. C. Burant, S. S. Iyengar, J. Tomasi, M. Cossi, J. M. Millam, M. Klene, C. Adamo, R. Cammi, J. W. Ochterski, R. L. Martin, K. Morokuma, O. Farkas, J. B. Foresman and D. J. Fox, Gaussian, Inc., Wallingford CT, 2016.

[S7] S. Kutsumizu, I. Tokiwa, A. Kawafuchi, Y. Miwa, Y. Yamamura and K. Saito, *Phys. Chem. Chem. Phys.*, **18**, 9013-9020 (2016).

[S8] T. Oka, Y. Yamamura, S. Kutsumizu and K. Saito, *Soft Matter*, **19**, 1194−1201 (2023).

[S9] S. Kutsumizu, A. Kawafuchi, Y. Yamamura, T. Udagawa, T. Otaki, M. Masuda, Y. Miwa and K. Saito, *Chem. Eur. J.*, **27**, 10293−10302 (2021).

[S10] S. Kutsumizu, Y. Yamada, T. Sugimoto, N. Yamada, T. Udagawa and Y. Miwa, *Phys. Chem. Chem. Phys.*, **20**, 7953–7961 (2018).